Ab initio molecular orbital/Rice–Ramsperger–Kassel–Marcus theory study of multichannel rate constants for the unimolecular decomposition of benzene and the $H+C_6H_5$ reaction over the ground electronic state

A. M. Mebel[a)]
Institute of Atomic and Molecular Sciences, Academia Sinica, Taipei, Taiwan 10764

M. C. Lin,[a)] D. Chakraborty, and J. Park
Department of Chemistry, Emory University, Atlanta, Georgia 30322

S. H. Lin and Y. T. Lee
Institute of Atomic and Molecular Sciences, Academia Sinica, Taipei, Taiwan 10764

(Received 6 September 2000; accepted 9 February 2001)

The potential energy surface for the unimolecular decomposition of benzene and $H+C_6H_5$ recombination has been studied by the *ab initio* G2M(cc, MP2) method. The results show that besides direct emission of a hydrogen atom occurring without an exit channel barrier, the benzene molecule can undergo sequential 1,2-hydrogen shifts to *o*-, *m*-, and *p*-C_6H_6 and then lose a H atom with exit barriers of about 6 kcal/mol. *o*-C_6H_6 can eliminate a hydrogen molecule with a barrier of 121.4 kcal/mol relative to benzene. *o*- and *m*-C_6H_6 can also isomerize to acyclic isomers, ac-C_6H_6, with barriers of 110.7 and 100.6 kcal/mol, respectively, but in order to form *m*-C_6H_6 from benzene the system has to overcome a barrier of 108.6 kcal/mol for the 1,2-H migration from *o*-C_6H_6 to *m*-C_6H_6. The bimolecular $H+C_6H_5$ reaction is shown to be more complicated than the unimolecular fragmentation reaction due to the presence of various metathetical processes, such as H-atom disproportionation or addition to different sites of the ring. The addition to the radical site is barrierless, the additions to the *o*-, *m*-, and *p*-positions have entrance barriers of about 6 kcal/mol and the disproportionation channel leading to *o*-benzyne$+H_2$ has a barrier of 7.6 kcal/mol. The Rice-Ramsperger-Kassel-Marcus and transition-state theory methods were used to compute the total and individual rate constants for various channels of the two title reactions under different temperature/pressure conditions. A fit of the calculated total rates for unimolecular benzene decomposition gives the expression $2.26\times10^{14}\exp(-53\,300/T)\,s^{-1}$ for $T=1000-3000$ K and atmospheric pressure. This finding is significantly different from the recommended rate constant, $9.0\times10^{15}\exp(-54\,060/T)\,s^{-1}$, obtained by kinetic modeling assuming only the $H+C_6H_5$ product channel. At $T=1000$ K, the branching ratios for the formation of $H+C_6H_5$ and ac-C_6H_6 are 29% and 71%, respectively. $H+C_6H_5$ becomes the major channel at $T\geqslant1200$ K. The total rate for the bimolecular $H+C_6H_5$ reaction is predicted to be between 4.5×10^{-11} and 2.9×10^{-10} $cm^3\,molecule^{-1}\,s^{-1}$ for the broad range of temperatures (300–3000 K) and pressures (100 Torr–10 atm). The values in the $T=1400-1700$ K interval, $\sim8\times10^{-11}\,cm^3\,molecule^{-1}\,s^{-1}$, are ~40% lower than the recommended value of $1.3\times10^{-10}\,cm^3\,molecule^{-1}\,s^{-1}$. The recombination reaction leading to direct formation of benzene through H addition to the radical site is more important than H disproportionations at $T<2000$ K. At higher temperatures the recombination channel leading to *o*-$C_6H_4+H_2$ and the hydrogen disproportionation channel become more significant, so *o*-benzyne$+H_2$ should be the major reaction channel at $T>2500$ K. © *2001 American Institute of Physics.* [DOI: 10.1063/1.1360201]

I. INTRODUCTION

Phenyl radicals play a vital role in the formation of polycyclic aromatic hydrocarbons (PAH's) and soots in hydrocarbon combustion under fuel rich conditions.[1] The reaction of the C_6H_5 radical with H atoms is directly relevant not only to the bimolecular association process, but also to the unimolecular decomposition of C_6H_6, a prototypical fragmentation process of aromatic compounds which has been investigated by many research groups,[2–10] including the UV photofragmentation reaction by Yokoyama *et al.*[10] The bimolecular reaction of H and C_6H_5 is, in fact, far more complicated than the unimolecular fragmentation reaction because of the presence of a wide variety of metathetical processes (such as H-atom disproportionation or addition to different sites on the ring).

In the present study, we explore all the possibilities of the interaction between H and C_6H_5, including the direct association, the disproportionation of H atoms from the *o*-, *m*-, and *p*-sites (from the radical center in C_6H_5), as well as addition to these sites followed by H-migration or ring-

[a)]Authors to whom correspondence should be addressed.

opening. The potential energy hypersurface (PES) encompassing these processes were computed at the G2M(cc,MP2)//B3LYP/6-31G(d,p) level of theory and the rate constants for the individual and/or directly coupled reactions have been calculated with transition-state theory (TST) or RRKM theory, wherever the method is applicable. For the reaction channel such as the direct association process producing C_6H_6 which does not have a well-defined TS, the maximum free energy criterion,[11] has been employed to estimate its TS structure variationally. The results of this detailed study are presented herein.

II. COMPUTATION METHODS

The geometries of various isomers of the benzene molecule, C_6H_5 and C_6H_4, as well as transition states for the $H+C_6H_5$ reaction and unimolecular decomposition of C_6H_6 have been optimized using the hybrid density functional B3LYP method[12] with the 6-31G(d,p) basis set.[13] Vibrational frequencies, calculated at the B3LYP/6-31G(d,p) level, have been used without scaling for characterization of stationary points, zero-point energy (ZPE) corrections and for RRKM calculations. All the stationary points have been positively identified for minimum (number of imaginary frequencies NIMAG=0) or transition state (NIMAG=1). All the energies quoted and discussed in the present paper include the ZPE corrections. For the singlet biradical structures such as transition states for the hydrogen addition to C_6H_5 to form cyclohexadienecarbene and for the H-disproportionation reaction, $H+C_6H_5 \rightarrow o\text{-}C_6H_4(^1A_1)+H_2$, we used the unrestricted singlet open shell UB3LYP method. This approach was recently shown to produce geometries for singlet biradicals, for instance, prefulvene[14] and planar allene,[15] in satisfactory agreement with multireference CASSCF calculations. We tested again the applicability of UB3LYP by comparison of the UB3LYP and CASSCF(10, 10) optimized geometries for one of the open shell singlet transition states.

In order to obtain more reliable energies we used the G2M(cc, MP2) (Ref. 16) method, a modification of the Gaussian-2 (G2) approach[17] by Pople and co-workers. It is targeted to approximate the coupled cluster[18] CCSD(T) calculation with the 6-311+G($3df,2p$) basis set with an additional empirical ''higher level correction'' (HLC). The total energy in G2M(cc, MP2) is calculated as follows:[16]

$$E[\text{G2M(cc,MP2)}] = E[\text{PMP4/6-311G}(d,p)] + \Delta E(\text{cc}) + \Delta E(+3df2p) + \Delta E(\text{HLC}) + \text{ZPE}[\text{B3LYP/6-31G}(d,p)],$$

where

$$\Delta E(\text{cc}) = E[\text{CCSD(T)/6-31G}(d,p)] - E[\text{PMP4/6-31G}(d,p)],$$

$$\Delta E(+3df2p) = E[\text{MP2/6-311+G}(3df,2p)] - E[\text{MP2/6-311G}(d,p)],$$

and the HLC is

$$\Delta E(\text{HLC}) = -5.05n_{\text{pair}} - 0.19n_{\text{un}},$$

where n_{pair} and n_{un} are the numbers of electron pairs and unpaired electrons, respectively. For the singlet biradical transition states the n_{pair} and n_{un} numbers were counted as for triplets. The accuracy expected from the G2M(cc, MP2) method is 1–2 kcal/mol both for minima and transition states. The GAUSSIAN 94 (Ref. 19) and MOLPRO 96 (Ref. 20) programs were employed for the calculations.

Rice–Ramsperger–Kassel–Marcus (RRKM) calculations have been carried out for the total and individual rate constants using the procedure described earlier,[21,22] based on a modified multichannel computer program initially written for the CH_3+O_2 reaction.[23]

III. RESULTS AND DISCUSSION

A. PES of the C_6H_6 system

Optimized geometries of various stable structures and transition states are shown in Figs. 1 and 2, respectively, and their energies and molecular parameters such as moments of inertia and vibrational frequencies are collected in Table I. Potential energy surfaces for the $H+C_6H_5$ reaction and for unimolecular decomposition of benzene are drawn in Fig. 3.

1. C_6H_6 decomposition

Let us first consider various channels associated with the unimolecular decomposition of C_6H_6. The benzene molecule can split out a hydrogen atom to produce the phenyl radical, C_6H_5. The calculated C–H bond strength in C_6H_6 is 115.2 kcal/mol at the G2M level, somewhat higher than the experimental value of 113–114 kcal/mol.[24] The H-elimination occurs without an intrinsic barrier. The second dissociation channel is the elimination of the hydrogen molecule leading to $o\text{-}C_6H_4$. This channel is less endothermic than C_6H_5+H, 86.1 kcal/mol, but has a high barrier. Initially, we searched for a transition state for the 1,2-H_2 elimination from benzene. However, the calculations converged to TS2 which is a transition state for the 1,1-H_2 elimination and connects the products, $o\text{-}C_6H_4(^1A_1)+H_2$, with the cyclohexadienecarbene intermediate **2** ($o\text{-}C_6H_6$). Thus, the H_2-elimination is preceded by the 1,2-H shift in **1** via TS1. We discussed TS1 and cyclohexadienecarbene earlier, in connection with the benzene-fulvene isomerization pathway.[14] TS1 and **2** lie 89.4 and 88.8 kcal/mol higher in energy than benzene, respectively. The barrier for the reverse **2**→TS1→**1** rearrangement is only 0.6 kcal/mol. TS2 is 32.6 kcal/mol higher than **2** and the overall barrier for the C_6H_6 **1**→$o\text{-}C_6H_4+H_2$ reaction is 121.4 kcal/mol. TS2 has a C_s symmetry with the forming H–H bond perpendicular to the plane of the C_6 ring. The transition state has a fairly late character; the H–H bond in H_2 is short, 0.84 Å. On the other hand, the breaking C–H bonds, 1.41 Å, are stretched by 28% as compared to those in cyclohexadienecarbene. For the $C_6H_6 \rightarrow TS1 \rightarrow \mathbf{2} \rightarrow TS2 \rightarrow o\text{-}C_6H_4+H_2$ channel, tunneling could be important at low temperatures since the barrier is high and the imaginary frequency in TS2 is also high, $\sim 1200i$ cm^{-1}, indicating a narrow barrier.

Interestingly, the H_2-elimination in benzene occurs in a similar manner as the 1,2-H_2 elimination in ethylene.[25] In C_2H_4 the 1,2-H_2 splitting has similar barrier heights and takes place stepwise; 1,2-H shift is followed by the

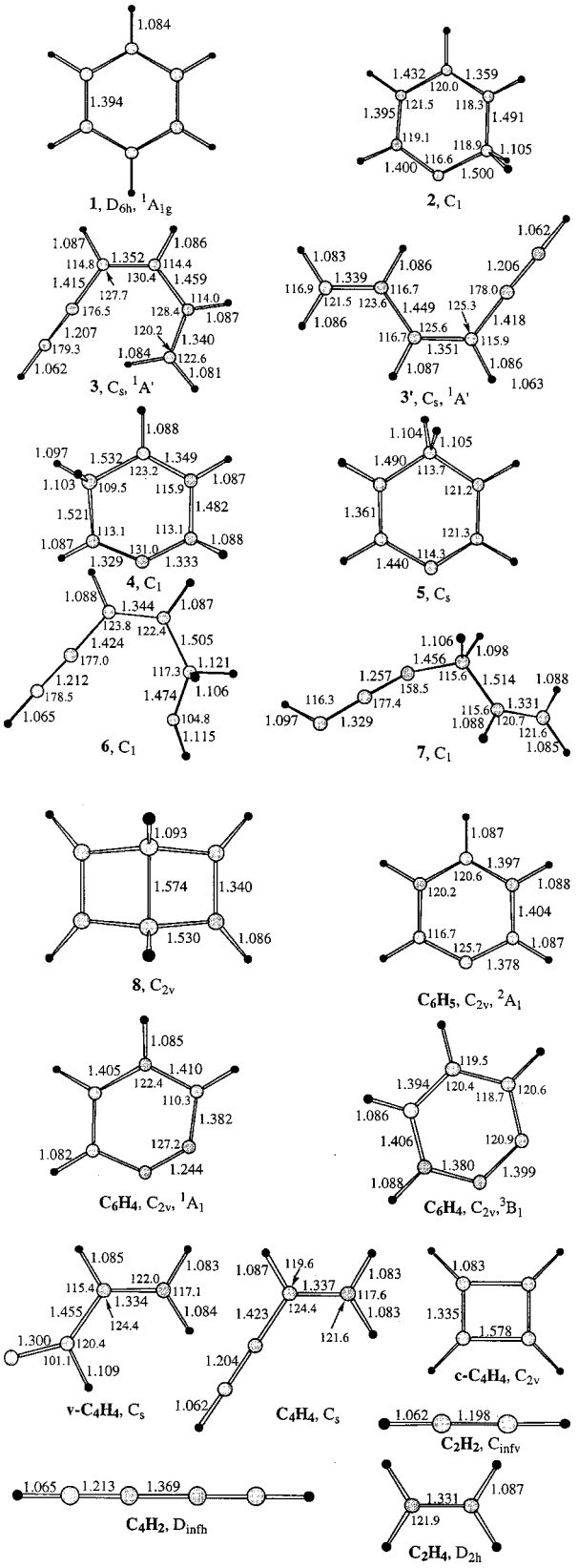

FIG. 1. Geometries of the reactants, products, and intermediates optimized at the B3LYP/6-31G(d,p) level. (Bond lengths are in Å, bond angles are degs.)

H_2-elimination. For instance, the reverse barrier from $CHCH_3$ to C_2H_4 is 1.2 kcal/mol (0.6 kcal/mol from cyclohexadienecarbene to benzene) and the barrier leading from $CHCH_3$ to $HCCH+H_2$ is 34.1 kcal/mol (compare with 32.6 kcal/mol for **2**→TS2→o-$C_6H_4+H_2$). There are some differences as well. The highest barrier on the C_2H_4→$CHCH_3$ →$HCCH+H_2$ pathway is 107.5 kcal/mol, significantly lower than that C_6H_6→**2**→o-$C_6H_4+H_2$, 121.4 kcal/mol. Also, the 1,2-H_2 elimination from ethylene is much less endothermic than that from benzene, 39.0 vs 86.1 kcal/mol. As a result, the barrier for the H_2-addition to acetylene is much higher, 68.5 kcal/mol, than that for o-C_6H_4, 35.3 kcal/mol.

Cyclohexadienecarbene **2** can isomerize or decompose by several other mechanisms. For instance, elimination of a H atom from the CH_2 group again gives the phenyl radical. The **2**→$H+C_6H_5$ reaction is endothermic by 26.4 kcal/mol with a barrier of 32.5 kcal/mol at TS3. TS3 is a late transition state; the breaking C–H bond is stretched to 1.83 Å and the structure of the C_6H_5 fragment resembles that of the phenyl radical. Accordingly, the transition state has a singlet open shell wave function with the $\mathbf{S}^2$ value of 1.02 and 1.48 at the UB3LYP and UHF levels, respectively, before annihilation of the first spin contaminant. The barriers for the H_2 and H eliminations in **2** are very close.

A ring opening in cyclohexadienecarbene leads to an acyclic isomer **3**, HC≡C–CH═CH–CH═CH_2, via TS4. The barrier at TS4 is calculated to be 110.7 kcal/mol relative to benzene. We discussed the structure of TS4 in detail earlier.[26] Mention only that in the **2**→TS4→**3** process the ring opening is accompanied by a 1,2-hydrogen shift. Structure **3** is 64.4 less stable than benzene. Another conformer of HC≡C–CH═CH–CH═CH_2, **3′**, obtained by a facile rotation around the single C–C bond, is slightly more favorable, 60.5 kcal/mol relative to **1**. The isomer **3** can also be readily formed by the isomerization **4**→**3** as shown in Fig. 3(a). In order to get to **4**(m-C_6H_6) from benzene, the system has to go through intermediate **2**, related to **4** by a 1,2-hydrogen migration. m-C_6H_6 lies 37.9 kcal/mol below the reactants but is 77.1 kcal/mol less stable than benzene **1**. **4** has no symmetry and can be described as cyclohexatriene (three double C═C bonds in the ring) rather than cyclohexadienecarbene. The barrier for the H-migration from CH_2 to CH at TS5 connecting **2** and **4** is found to be quite low, 19.8 and 108.6 kcal/mol with respect to **2** and **1**, respectively. In the isomerization reaction **4**→**3** via transition state TS6 the breaking C–C bond between CH_2 and CH is elongated to 2.034 Å. The barrier for ring opening is relatively low, 23.3 kcal/mol with respect to **4**. The energy of TS6 with respect to benzene is 100.6 kcal/mol, i.e., 10.1 kcal/mol lower than the energy of TS4, the transition state for ring opening in **2** accompanied with a hydrogen shift. The ring-opening in benzene can occur by the following pathway: **1**→TS1→**2**→TS5→**4** →TS6→**3** or **3′** with the highest barrier of 108.6 kcal/mol at TS5. The other pathways leading to the ring-opening have slightly higher but comparable barriers: **1**→TS1→**2**→TS4 (110.7 kcal/mol)→**3** or **3′** and **1**→···→fulvene→hydrogen shift→ring opening (111.3 kcal/mol)→H_2C═C═CH–CH═C═CH_2.[26]

ac-C_6H_6 (**3** and **3′**) can eventually produce $C_4H_4+C_2H_2$ and $C_4H_2+C_2H_4$ by various mechanisms illustrated in Fig. 3(b). In the first mechanism, the initial step is a 1,2-H migration via TS7 to produce vinylvinylidene v-C_4H_4 and

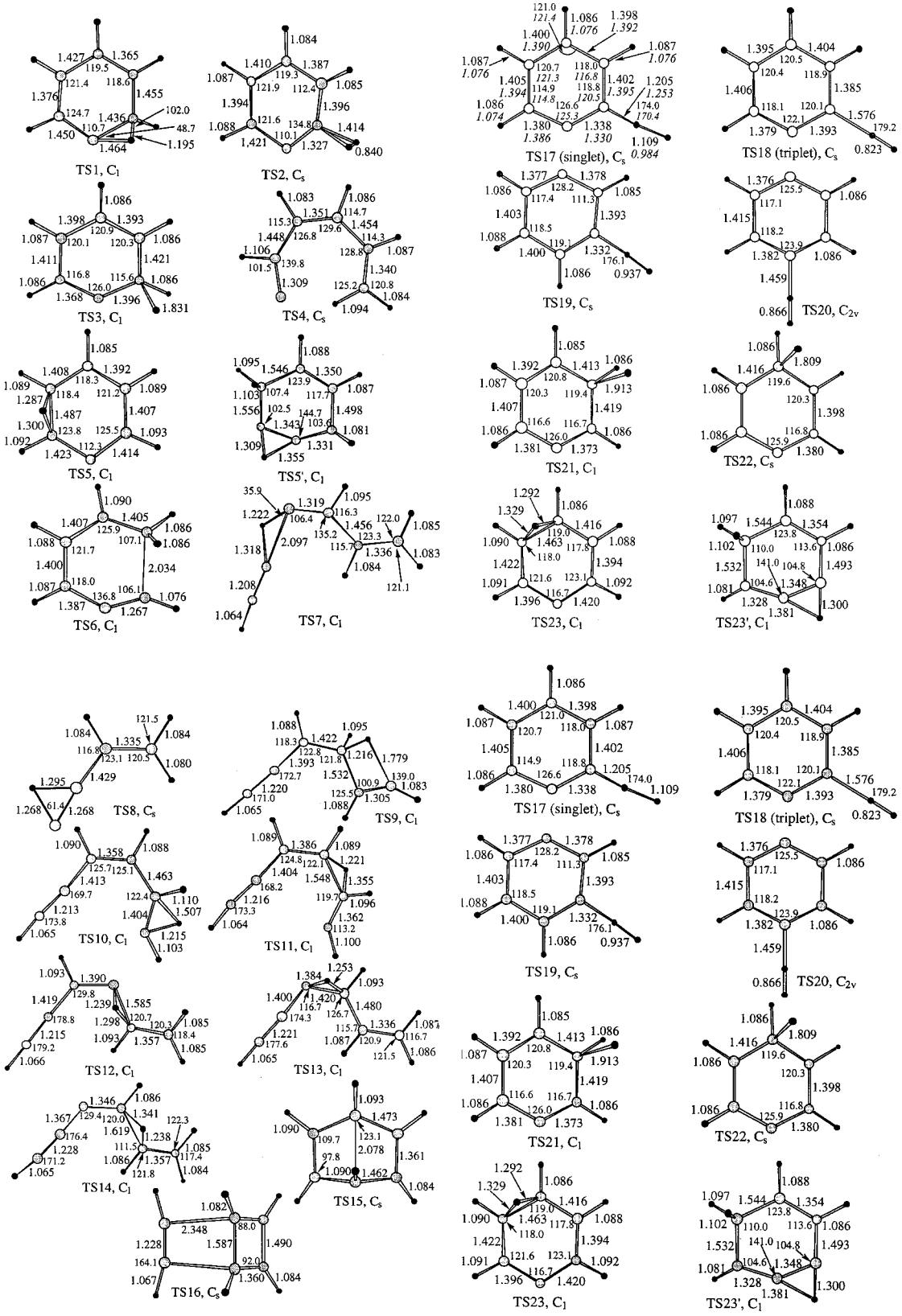

FIG. 2. Geometries of transition states optimized at the B3LYP/6-31G(d,p) level. (Bond lengths are in Å, bond angles are degs.)

C_2H_2. In TS7, the forming and breaking C–H bond lengths are 1.318 and 1.222 Å, respectively, and the breaking C–C bond is stretched to 2.10 Å. The H-migration has a very high barrier, 103.8 and 164.3 kcal/mol above **3′** and **1**, respectively. The intermediate, v-C_4H_4, which lies 139.0 kcal/mol higher than benzene has a singlet carbene structure and can undergo H-migration to the more stable vinylacetylene C_4H_4 isomer with a barrier of 4.1 kcal/mol via TS8. The calculated

TABLE I. Relative energies at the G2M(cc,MP2) level and molecular and transition-state parameters at the B3LYP/6-31G** level of the reactants, products, and transition states for the reactions of unimolecular decomposition of benzene and C_6H_5+H.

Species	E_{rel} (kcal/mol)	i	I_i (10^{-40} g cm^2)	ν_j (cm^{-1})
C_6H_6 **1**	0.0	A	148.0	412,412,623,623,687,723,861,861,980,980,
		B	148.0	1014,1016,1023,1061,1061,1175,1198,1198,
		C	296.1	1336,1382,1513,1513,1638,1638,3155,3165,
				3165,3180,3180,3191
o-C_6H_6 **2**	88.2	A	149.3	165,229,415,546,578,709,810,817,886,915,
		B	158.5	966,979,991,1037,1149,1185,1191,1271,
		C	299.4	1312,1377,1402,1435,1521,1634,2978,3009,
				3138,3154,3168,3196
ac-C_6H_6 **3**	64.4	A	132.4	51,152,277,292,458,464,636,673,676,759,
		B	304.6	791,863,957,993,1019,1037,1106,1270,
		C	436.9	1351,1438,1466,1630,1683,2188,3128,3137,
				3151,3160,3245,3476
ac-C_6H_6 **3′**	60.5	A	84.27	127,143,267,306,429,469,629,680,692,717,
		B	435.5	809,895,943,987,988,1046,1167,1265,1319,
		C	519.7	1396,1468,1626,1685,2193,3132,3140,3154,
				3160,3222,3477
m-C_6H_6 **4**	77.3	A	143.5	230,379,448,503,589,696,757,805,852,867,
		B	161.5	929,965,988,1005,1157,1164,1179,1299,
		C	287.3	1303,1372,1425,1460,1621,1828,2988,3061,
				3163,3169,3171,3191
p-C_6H_6 **5**	92.9	A	150.3	233,291,460,527,552,709,777,884,899,939,
		B	157.1	957,982,1018,1018,1144,1170,1218,1279,
		C	299.3	1364,1410,1428,1437,1545,1607,2969,2995,
				3135,3136,3162,3162
C_6H_6 **6**	144.7	A	144.4	79,100,230,287,433,471,584,587,632,651,
		B	275.6	709,773,890,975,992,1007,1150,1167,1238,
		C	397.6	1338,1384,1427,1685,2212,2857,2898,2953,
				3164,3189,3490
C_6H_6 **7**	131.4	A	64.9	33,82,169,290,326,402,454,564,617,814,845,884,
		B	535.5	938,951,1029,1120,1204,1308,1331,1379,1422,
		C	577.0	1462,1725,2005,2970,3044,3092,3152,3176,3240
C_6H_6 **8**	77.9	A	107.7	338,393,491,727,790,818,836,876,934,934,949,
		B	190.3	961,966,1004,1044,1107,1170,1188,1210,1218,
		C	243.9	1300,1309,1620,1647,3102,3108,3189,3191,
				3219,3222
$C_6H_5(+H)$	115.2	A	134.8	401,428,601,619,672,722,815,890,958,986,
		B	151.0	988,1023,1058,1081,1182,1183,1313,1342,
		C	285.7	1473,1485,1592,1646,3173,3179,3192,3194,
				3205
o-C_6H_4 $^1A_1$	86.1	A	120.1	395,427,451,604,626,751,848,869,923,971,
$(+H_2)$		B	147.6	999,1064,1108,1162,1271,1306,1424,1468,
		C	267.6	1482,2013,3158,3174,3195,3198
o-C_6H_4 $^3B_1$	127.3	A	129.4	399,417,587,602,606,730,797,923,968,977,
$(+H_2)$		B	144.0	1022,1056,1112,1177,1225,1324,1443,1450,
		C	273.4	1571.1626,3168,3171,3186,3201
C_4H_4	101.1	A	16.6	224,317,560,647,679,703,893,955,1011,
$(+C_2H_2)$		B	176.4	1111,1321,1444,1668,2205,3135,3147,3236,
		C	193.0	3478
v-C_4H_4	139.0	A	15.6	145,176,423,537,742,853,932,943,1017,
$(+C_2H_2)$		B	175.0	1162,1329,1443,1668,1776,2967,3142,
		C	190.6	3170,3231
c-C_4H_4	136.7	A	49.7	542,590,595,712,846,854,877,963,1069,
$(+C_2H_2)$		B	66.2	1119,1186,1271,1644,1656,3210,3226,
		C	115.9	3248,3259
C_4H_2	102.7	A	191.4	235,235,527,527,662,662,662,662,917,
$(+C_2H_4)$		B	191.4	2110,2284,3477,3479
TS1	89.4	A	149.7	762*i*,233,379,589,614,672,686,813,895,921,
		B	153.3	987,1005,1022,1035,1047,1180,1200,1239,
		C	299.0	1259,1398,1449,1477,1556,1659,2334,3125,
				3141,3164,3178,3201
TS2	121.4	A	145.9	1198*i*,303,400,471,554,650,651,741,802,
		B	151.7	817,884,934,941,1002,1010,1041,1129,
		C	295.9	1171,1192,1263,1363,1426,1478,1565,1661,
				3114,3148,3159,3169,3189

TABLE I. (*Continued.*)

Species	E_{rel} (kcal/mol)	i	I_i (10^{-40} g cm^2)	ν_j (cm^{-1})
TS3	121.4	A	142.5	887*i*,295,342,434,487,593,614,682,733,835,
		B	161.9	920,972,980,1008,1019,1048,1063,1173,
		C	294.0	1180,1301,1336,1456,1475,1566,1626,3176,
				3182,3191,3195,3205
TS4	110.7	A	147.9	96*i*,174,217,329,417,444,589,702,741,803,
		B	232.3	872,913,987,996,1016,1019,1104,1270,
		C	380.2	1138,1442,1483,1613,1689,1734,2969,2988,
				3132,3155,3183,3186
TS5	108.6	A	149.5	1022*i*,286,368,574,620,666,712,843,901,
		B	152.4	920,963,1016,1033,1057,1064,1156,1190,
		C	297.9	1208,1309,1345,1412,1446,1550,1592,2173,
				3107,3120,3154,3158,3212
TS6	100.6	A	161.0	554*i*,255,374,444,519,569,645,689,771,805,
		B	166.3	889,972,987,1001,1044,1100,1124,1202,
		C	319.6	1268,1412,1477,1500,1557,1894,3115,3145,
				3166,3181,3191,3322
TS7	164.3	A	124.1	1211*i*,93,95,136,205,295,353,464,621,670,
		B	415.2	703,728,775,853,927,951,1032,1133,1222,
		C	539.3	1315,1439,1621,1683,2060,2228,3069,3138,
				3179,3226,3445
TS8	143.1	A	19.3	382*i*,92,285,219,628,669,869,944,997,1096,
($+C_2H_2$)		B	168.3	1321,1443,1666,1952,2377,3153,3180,3253
		C	187.7	
TS9	153.1	A	89.6	984*i*,118,169,280,364,423,482,585,632,636,
		B	406.1	665,723,771,878,893,982,1061,1152,1172,
		C	469.7	1289,1310,1449,1689,2100,2160,3073,3164,
				3170,3247,3485
TS10	159.6	A	136.0	1337*i*,91,151,231,282,418,496,544,606,648,
		B	295.4	734,797,857,912,984,1007,1036,1186,1239,
		C	416.2	1328,1438,1459,1640,2204,2227,2873,3031,
				3151,3177,3493
TS11	179.5	A	140.4	1111*i*,115,155,220,357,432,496,523,563,658,
		B	276.2	712,783,789,935,969,976,1029,1148,1202,
		C	398.8	1271,1367,1441,1576,2175,2264,3042,3075,
				3154,3169,3495
TS12	164.6	A	98.7	1218*i*,114,134,241,298,419,492,517,602,627,
		B	404.1	670,686,837,916,946,988,1028,1046,1283,
		C	497.4	1301,1383,1460,1592,2174,2252,3108,3113,
				3170,3269,3483
TS13	135.2	A	90.9	1012*i*,107,131,250,311,360,442,487,677,705,
		B	416.0	728,837,884,965,970,1042,1171,1262,1319,
		C	502.3	1363,1403,1482,1711,2120,2162,3108,3154,
				3185,3243,3490
TS14	164.6	A	85.1	1149*i*,105,154,220,260,320,432,514,540,623,
		B	449.6	708,715,807,871,939,966,1054,1211,1306,
		C	527.6	1347,1424,1559,1624,2077,2149,3171,3191,
				3207,3266,3481
TS15	103.5	A	120.0	478*i*,347,428,568,591,718,721,794,842,859,
		B	174.8	884,906,993,1067,1104,1120,1124,1190,1301,
		C	257.8	1355,1357,1416,1554,1571,3109,3135,3137,
				3143,3218,3222
TS16	147.5	A	121.4	449*i*,156,196,219,313,570,598,610,641,682,
		B	260.0	709,746,793,853,862,897,1004,1051,1153,
		C	313.2	1197,1305,1496,1577,1942,3209,3226,3246,
				3259,3405,3482
TS17	122.8	A	136.6	1169*i*,237,320,413,445,594,615,653,747,
		B	170.9	848,923,935,979,1001,1023,1059,1101,
		C	307.5	1177,1184,1291,1350,1416,1487,1496,1575,
				1688,3175,3183,3197,3204
TS18	134.3	A	298.9	686*i*,153,185,398,421,583,602,629,734,812,
		B	372.3	874,929,957,968,980,1021,1056,1118,1178,
		C	671.2	1235,1326,1451,1453,1572,1629,2758,3171,
				3176,3187,3201

TABLE I. (*Continued.*)

Species	E_{rel} (kcal/mol)	i	I_i (10^{-40} g cm^2)	ν_j (cm^{-1})
TS19	126.1	A	138.6	1172*i*,229,279,407,467,569,593,634,768,
		B	169.3	843,876,912,973,1008,1017,1041,1094,
		C	307.8	1165,1182,1290,1334,1420,1438,1549,1612, 1673,3169,3193,3202,3205
TS20	132.3	A	151.3	959*i*,197,254,408,443,592,602,639,765,771,
		B	158.9	923,930,944,970,1020,1053,1068,1117,
		C	310.1	1166,1287,1301,1403,1465,1470,1645,2169, 3183,3185,3198,3199
TS21	121.4	A	142.6	710*i*,286,356,404,459,594,613,665,743,819,
		B	162.3	878,967,981,1002,1016,1053,1067,1170,
		C	293.7	1180,1306,1339,1458,1480,1558,1623,3176, 3183,3195,3197,3207
TS22	121.6	A	146.3	885*i*,303,377,440,457,595,612,652,756,810,
		B	157.4	927,954,981,998,1047,1051,1074,1169,
		C	293.3	1180,1314,1322,1462,1474,1574,1607,3177, 3183,3191,3197,3203
TS23	114.1	A	147.2	1154*i*,221,373,548,599,646,693,847,861,
		B	154.0	917,955,988,1038,1050,1081,1135,1194,
		C	294.9	1221,1342,1391,1428,1452,1513,1548,2107, 3111,3118,3142,3165,3202

endothermicity of the $C_6H_6 \rightarrow C_4H_4+C_2H_2$ reaction is 101.1 kcal/mol. Vinylacetylene can be also produced directly from **3′** by a 1,3-H migration via TS9. In this case, the barrier is somewhat lower, 92.6 and 153.1 kcal/mol relative to ac-C_6H_6 and benzene, respectively. A stepwise mechanism involving two sequential 1,2-hydrogen shifts leads from **3** to $C_4H_4+C_2H_2$ via a carbene intermediate **6**, CH≡C–CH═CH–CH_2–CH. The highest barrier occurs at the second step at TS11 which lies 179.3 kcal/mol above **1**. Thus, among the three mechanisms for the formation of vinylacetylene from ac-C_6H_6, the most favorable one is **3′** $\rightarrow$TS9$\rightarrow C_4H_4+C_2H_2$ with the barrier of 153.1 kcal/mol with respect to benzene. Hence, we do not expect that the $C_4H_4+C_2H_2$ product channel is able to compete with the production of H or H_2 from the unimolecular decomposition of benzene even at high temperatures.

ac-C_6H_6 can also decompose to C_4H_2 (ethynylacetylene) and ethylene. The overall endothermicity for the C_6H_6 **1** $\rightarrow C_4H_2+C_2H_4$ channel, 102.7 kcal/mol, is similar to that for $C_4H_4+C_2H_2$. **3′** can undergo a 1,2-H shift at TS12 accompanied with a rupture of the bridged CC bond. The barrier is 164.6 and 104.1 kcal/mol relative to **1** and **3′**, respectively. It seems that ethynylvinylidene should be produced instead of ethynylacetylene after the barrier at TS12 is cleared. However, both B3LYP/6-31G(d,p) and MP2/6-31G(d,p) optimization showed that ethynylvinylidene is not a local minimum on the potential energy surface of C_4H_2 and it spontaneously rearranges to ethynylacetylene. Therefore, we conclude that TS12 connects **3′** with the C_4H_2 (ethynylacetylene)$+C_2H_4$ products. Second possible channel leading to the same products, **3′**$\rightarrow$TS13$\rightarrow$**7**$\rightarrow$TS14 $\rightarrow C_4H_2+C_2H_4$, involves two sequential 1,2-H migrations via the carbene intermediate **7**, CH–C≡C–CH_2–CH═CH_2. The higher barrier is found at TS14 and it is similar to that at TS12, 164.6 kcal/mol above benzene. Despite a careful search, we failed to locate a transition state connecting ac-C_6H_6 with $C_4H_2+C_2H_4$ via a 1,3-hydrogen shift similar to TS9 for the $C_4H_4+C_2H_2$ products. The optimizations always converged to TS13 or TS14 indicating that in this case two sequential 1,2-H shifts are preferable to a 1,3-H shift. Thus, the barrier to produce $C_4H_2+C_2H_4$ from benzene is 11.5 kcal/mol higher than that for production $C_4H_4+C_2H_2$.

There exist other numerous channels of isomerization among **2**, **3**, and **3′**. We discussed them in our earlier works.[14,26] For example, **2** can rearrange to fulvene by a two-step mechanism with the highest barrier of 104.7 kcal/mol relative to benzene.[14] Isomerization of **3** and **3′** can occur by sequential hydrogen shifts and lead to the dissociation to $2C_3H_3$ or $C_5H_3+CH_3$.[26] However, these two product channels are about 150 kcal/mol endothermic and not expected to compete with much more favorable C_6H_5+H or *o*-$C_6H_4+H_2$ dissociation. Fulvene can, in principle, eliminate the CH_2 group giving $C_5H_4+CH_2$ and **3** and **3′** could produce $C_2H_3+C_4H_3$. We anticipate that these two channels are not significant in benzene decomposition due to their high endothermicity, similar to those for $2C_3H_3$ or $C_5H_3+CH_3$.

Interestingly, an excited isomer of C_4H_4, cyclobutadiene *c*-C_4H_4, can be formed from benzene with a slightly lower barrier than the more stable vinylacetylene. The pathway to *c*-C_4H_4 involves the isomerization of benzene **1** to Dewar benzene **8** via TS15 with a barrier of 103.5 kcal/mol. At the second step, Dewar benzene (77.9 kcal/mol higher in energy than **1**) decomposes to *c*-C_4H_4 and acetylene with the barrier of 69.6 kcal/mol at TS16. The highest barrier at TS16 is 147.5 kcal/mol relative to benzene, i.e., 5.6 kcal/mol lower than the barrier at TS9 leading to vinylacetylene. Meanwhile,

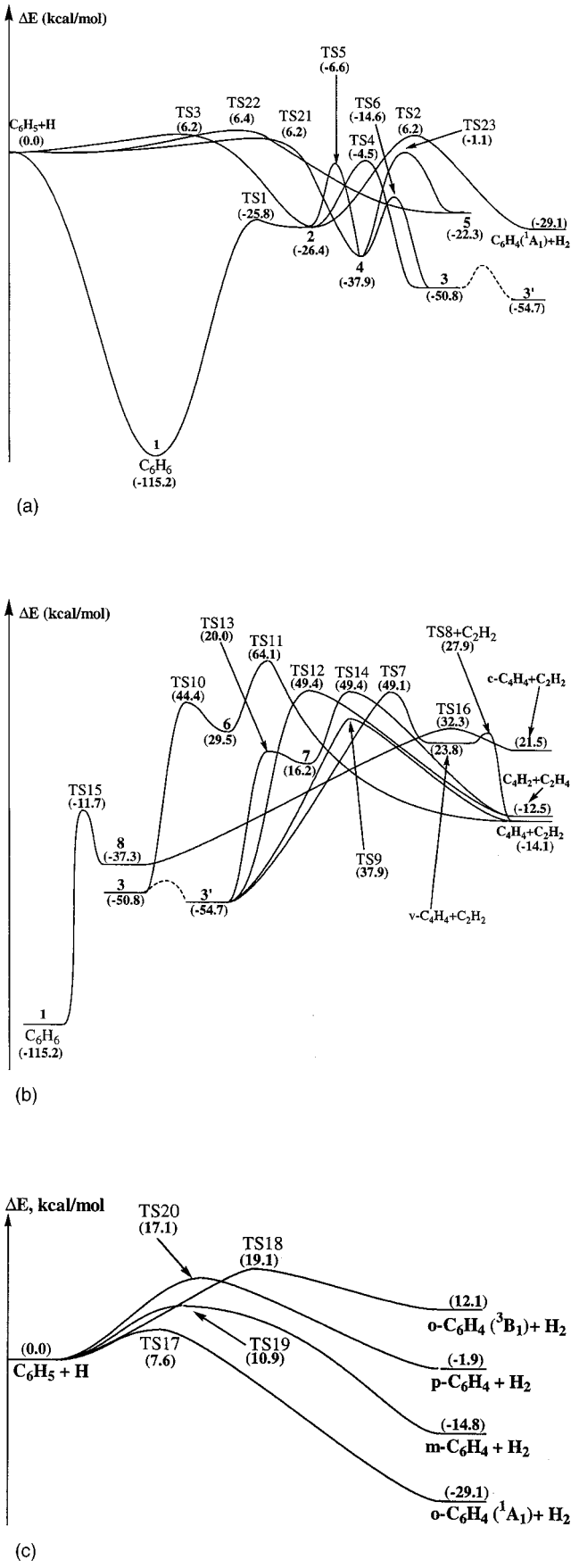

FIG. 3. Potential energy diagram for the bimolecular $H+C_6H_5$ reaction and for unimolecular decomposition of benzene calculated at the G2M(cc, MP2) level: (a) the channels common for the two reactions; (b) the channels leading to the $C_4H_4+C_2H_2$ and $C_4H_2+C_2H_4$ products; (c) the H-disproportionation processes accessible for $H+C_6H_5$.

the calculated endothermicity for the C_6H_6 **1** $\rightarrow c\text{-}C_4H_4+C_2H_2$ reaction is 136.7 kcal/mol.

2. Bimolecular $H+C_6H_5$ reaction

According to the potential energy diagram shown in Fig. 3, several channels for the $H+C_6H_5$ reaction are feasible. Some are the reverse of the unimolecular reaction mentioned above, some are not directly accessible, such as the H-disproportionation processes. H-association with C_6H_5 at the radical site should dominate the reaction, at least at low temperatures since the pathway does not have a barrier and is highly exothermic. H-addition to the ortho-position to give cyclohexadienecarbene ($o\text{-}C_6H_6$ **2**) is exothermic by 26.3 kcal/mol and proceeds via an early transition state TS3 with a barrier of 6.1 kcal/mol. Intermediate **2** would rapidly isomerize to benzene. The other two reaction pathways involve H-disproportionation to produce H_2 and *o*-benzyne in the singlet or triplet state [see Fig. 3(c)]. The singlet reaction is calculated to be exothermic by 29.1 kcal/mol and to have a barrier of 7.6 kcal/mol at TS17. Similar to TS3, TS17 has a strong biradical character; the computed $\mathbf{S}^2$ value before annihilation is 0.81 and 1.67 at the UB3LYP/6-31G** and UHF/6-31G** levels, respectively. In accord with the reaction exothermicity, TS17 has an early character; the forming H–H bond is 1.11 Å, about 50% longer than the regular H–H bond in H_2, while the breaking C–H bond is only 11% longer than such bond in the phenyl radical. To check the applicability of the UB3LYP method to geometry optimization of such an open shell singlet transition state, we additionally optimized TS17 at the CASSCF(10,10)/6-31G** level. All geometric parameters obtained at UB3LYP and CASSCF(10,10) are very close, except the breaking C–H (1.253 vs 1.205 Å) and forming H–H (0.984 vs 1.109 Å) bond lengths. The barrier height computed at the G2M level with the CASSCF optimized geometry of TS17 is 8.5 kcal/mol. Thus, despite of the notable difference in some geometric parameters, the difference in energies computed at the higher level of theory is less than 1 kcal/mol, indicating that the G2M//UB3LYP is a reasonable alternative for time-consuming CASSCF calculations. The energetics of the $H+C_6H_5\rightarrow o$-benzyne$+H_2$ reaction is quite different from that of $H+C_6H_6\rightarrow C_6H_5+H_2$. The former is exothermic and requires relatively low activation energy, while the latter was found to be endothermic by 11.1 kcal/mol and has a high barrier of 19.9 kcal/mol.[27] Also, the phenyl radical is much more reactive with respect to H_2 as compared with $o\text{-}C_6H_4$. The barrier for the $C_6H_5+H_2\rightarrow C_6H_6+H$ hydrogen disproportionation reaction is 8.8 kcal/mol (Ref. 27) vs 36.7 kcal/mol for $o\text{-}C_6H_4(^1A_1)+H_2\rightarrow H+C_6H_5$.

The H-disproportionation on the triplet surface, $H+C_6H_5\rightarrow o\text{-}C_6H_4(^3B_1)+H_2$, is found to be endothermic (12.1 kcal/mol) and has a higher barrier of 19.1 kcal/mol at TS18. TS18 has quite a different geometry as compared with TS17. The transition state is late with a short H–H distance of 0.82 Å and a long breaking C–H bond of 1.58 Å. Due to the higher activation energy, the triplet *o*-benzyne channel is not expected to be competitive with the singlet channel for the $H+C_6H_5$ reaction.

In experiment,[28] the *m*- and *p*-isomers of benzyne are 15.3 and 30.7 kcal/mol less stable than *o*-C_6H_4. Their relative energies with regard to *o*-C_6H_4 are 14.3 and 27.2 kcal/mol, respectively, at the CCSD(T)/aANO level[28(c)] comparable with our theoretical method. Similar values were obtained recently at the G2M(rcc, MP2) level.[28(d)] Using these numbers, we can estimate the exothermicities of the *m*-$C_6H_4+H_2$ and *p*-$C_6H_4+H_2$ channels of the $H+C_6H_5$ reaction as 14.8 and 1.9 kcal/mol, respectively. The H-disproportionation from the *m*- and *p*-sites in C_6H_5 goes through transition states TS19 and TS20, respectively. The reactions are significantly less exothermic than the H-disproportionation from the *o*-site and this results in the barrier increase and later character of the transition states relative to $H+C_6H_5$. For instance, the *m*-disproportionation barrier is 10.9 kcal/mol, 3.3 kcal/mol higher than that for *o*-disproportionation. In TS19, the breaking C–H bond distance is 1.332 Å cf. with 1.209 Å in TS17. The forming H–H bond length in TS19 is 0.937 Å, 0.172 Å shorter than that in TS17. The barrier for *p*-disproportionation is even higher, 17.1 kcal/mol at the G2M level and transition state TS20 is rather late, with the C–H and H–H distances of 1.459 and 0.866 Å, respectively. Similar to TS17, TS19 and TS20 possess an open shell singlet character. Interestingly, Logan and Chen calculated a barrier for hydrogen disproportionation from the CH_3 group in methanol by *p*-C_6H_4 to be 9.5 kcal/mol.[29] The present calculations give a higher barrier for the *p*-$C_6H_4+H_2\rightarrow C_6H_5+H$ reaction, ~19 kcal/mol. Summarizing, we can conclude that the channels leading to *p*- and *m*-benzynes should be slower than *o*-$C_6H_4+H_2$. Of these three C_6H_4 channels, the latter is expected to compete with the hydrogen addition via TS3.

Addition of the hydrogen atom can also occur to the *m*- or *p*-site of the phenyl radical. Meta-addition gives intermediate **4**(*m*-C_6H_6). According to the higher exothermicity for the formation of **4** as compared to **2** (*o*-addition), the corresponding transition state TS21 has an earlier character than TS3 which is reflected in the longer C–H distance, 1.913 Å, for the forming bond. However, both transition states TS3 and TS21 have similar energies, 6.2 kcal/mol relative to $H+C_6H_5$. Addition to the *p*-position gives C_s-symmetric intermediate **5** (cyclohexadiene *p*-C_6H_6) where the carbon atoms form a boat configuration of the C_6 ring. **5** is the least stable isomer among the cyclohexadienecarbenes; it lies 22.3 kcal/mol below C_6H_5+H or 92.9 kcal/mol higher than benzene. The transition state connecting the reactants with **5** is TS22. It has the latest character as compared to TS3 and TS21, with the forming C–H bond distance of 1.809 Å. Meanwhile, the energetic barrier for the *p*-addition, 6.4 kcal/mol, is only 0.2 kcal/mol higher than the barriers for *o*- and *m*-addition.

When **4** is formed by H-addition to the *m*-position of C_6H_5, two channels can compete for rearrangement of this intermediate: **4**→TS6→**3** and **4**→TS5→**2**→TS1→**1**, as described in the preceding section. The ring-opening in **4** is more favorable since the barrier at TS6 is 8 kcal/mol lower than that at TS5. Interestingly, there exists another transition state TS5′ connecting **4** and **2** via a 1,2-H shift from CH to the hydrogenless carbon. However, in this case the barrier is very high, 68.4 kcal/mol with respect to **4**.

Intermediate **5** can also undergo a hydrogen shift from CH_2 to CH to form **4** with a low barrier of 21.2 kcal/mol at TS23 or the H-shift from CH to C with a high barrier of 49.8 kcal/mol at TS23′. Thus, **5** can eventually isomerize to benzene, **5**→TS23→**4**→TS5→**2**→TS1→**1**, or to the chain structure ac-C_6H_6, **5**→TS23→**4**→TS6→**3** or **3**′. Direct ring-opening in **5** is unlikely since it would result in a high energy carbene chain structure. The three channels of hydrogen addition to the phenyl radical, to the *o*-, *m*-, and *p*-positions, are seemingly feasible and can interact with each other through hydrogen shifts in **2**, **4**, and **5**, because the energies of TS5 and TS23 are lower than that of $H+C_6H_5$.

B. RRKM calculations of rate constants for key product channels

1. C_6H_6 decomposition

The rate constant for the unimolecular decomposition of C_6H_6 was calculated with the following scheme based on the PES discussed in the preceding section:

$$
\begin{aligned}
C_6H_6 \underset{+M(-a)}{\overset{+M(a)}{\rightleftarrows}} C_6H_6^{\dagger} &\xrightarrow{b} H+C_6H_5 \\
&\underset{-c}{\overset{c}{\rightleftarrows}} o-C_6H_6^{\dagger} \xrightarrow{d} H+C_6H_5 \\
&\xrightarrow{e} H_2+C_6H_4 \\
&\underset{-f}{\overset{f}{\rightleftarrows}} m\text{-}C_6H_6^{\dagger} \underset{-g}{\overset{g}{\rightleftarrows}} \text{ac-}C_6H_6^{\dagger} \xrightarrow[+M]{j} \text{ac-}C_6H_6 \\
&\xrightarrow{h} m\text{-}C_6H_6(+M) \\
&\xrightarrow{i} H+C_6H_5(\text{or } p\text{-}C_6H_6+M).
\end{aligned}
$$

TABLE II. Calculated total and individual rate constants for benzene decomposition and isomerization (s^{-1}) at various pressures.

T,(K)	k_{tot}	$k(C_6H_5+H)$[a]	$k(C_6H_4+H_2)$	$k(m\text{-}C_6H_6)$	$k(ac\text{-}C_6H_6)$	k_{iso}[b]
			$P=760$ Torr			
1000	9.01×10^{-10}	2.64×10^{-10}	1.06×10^{-12}	7.87×10^{-11}	5.57×10^{-10}	6.36×10^{-10}
1500	1.59×10^{-1}	8.86×10^{-2}	1.26×10^{-3}	6.17×10^{-4}	6.81×10^{-2}	6.87×10^{-2}
2000	1.64×10^{3}	1.13×10^{3}	2.55×10^{1}	8.16×10^{-1}	4.85×10^{2}	4.86×10^{2}
2500	1.67×10^{5}	1.29×10^{5}	3.32×10^{3}	3.05×10^{1}	3.46×10^{4}	3.46×10^{4}
3000	1.16×10^{6}	9.96×10^{5}	2.57×10^{4}	9.62×10^{1}	1.43×10^{5}	1.43×10^{5}
			$P=10$ atm			
1000	9.04×10^{-10}	2.64×10^{-10}	1.06×10^{-12}	3.03×10^{-10}	3.36×10^{-10}	6.39×10^{-10}
1500	1.63×10^{-1}	9.13×10^{-2}	1.34×10^{-3}	4.91×10^{-3}	6.58×10^{-2}	7.07×10^{-2}
2000	2.25×10^{3}	1.54×10^{3}	4.03×10^{1}	6.54×10^{0}	6.56×10^{2}	6.63×10^{2}
2500	3.95×10^{5}	2.95×10^{5}	9.67×10^{3}	2.41×10^{2}	8.99×10^{4}	9.01×10^{4}
3000	4.76×10^{6}	3.83×10^{6}	1.30×10^{5}	1.05×10^{3}	8.05×10^{5}	8.06×10^{5}
			$P=100$ Torr			
1000	8.99×10^{-10}	2.63×10^{-10}	1.06×10^{-12}	1.44×10^{-11}	6.20×10^{-10}	6.34×10^{-10}
1500	1.44×10^{-1}	8.06×10^{-2}	1.05×10^{-3}	9.94×10^{-5}	6.19×10^{-2}	6.20×10^{-2}
2000	9.69×10^{2}	6.90×10^{2}	1.27×10^{1}	1.72×10^{-1}	2.66×10^{2}	2.66×10^{2}
2500	5.88×10^{4}	4.83×10^{4}	9.70×10^{2}	4.99×10^{0}	9.56×10^{3}	9.56×10^{3}
3000	2.73×10^{5}	2.48×10^{5}	4.92×10^{3}	9.54×10^{0}	2.08×10^{4}	2.08×10^{4}

[a] $k(C_6H_5+H)$ is the sum of k_b, k_d, and k_i but 99% of the rate derived from direct dissociation given by k_b.
[b] $k_{iso}=k(m\text{-}C_6H_6)+k(ac\text{-}C_6H_6)$.

Steady-state treatment for the collisional activated C_6H_6 isomers: $C_6H_6^{\dagger}$, $o\text{-}C_6H_6^{\dagger}$, $m\text{-}C_6H_6^{\dagger}$, and $ac\text{-}C_6H_6^{\dagger}$ leads to the following expressions for the individual processes:

$C_6H_6 \rightarrow H+C_6H_5$:

$$k_b = l_b^{\neq} I_r \frac{kT}{h} \frac{e^{-E_b^o/RT}}{Q_{C_6H_6}} \int_0^{\infty} \frac{\omega_1 \Sigma P_b(E^{\neq})}{AB} e^{-E^{\neq}/RT} d\left(\frac{E^{\neq}}{RT}\right),$$

$C_6H_6 \rightarrow o\text{-}C_6H_6 \rightarrow H+C_6H_5$:

$$k_d = l_c^{\neq} I_r \frac{kT}{h} \frac{e^{-E_b^o/RT}}{Q_{C_6H_6}} \times \int_0^{\infty} \frac{\omega_1 k_d(E) \Sigma P_c(E^{\neq})}{AB \cdot BA} e^{-E^{\neq}/RT} d\left(\frac{E^{\neq}}{RT}\right),$$

$C_6H_6 \rightarrow o\text{-}C_6H_6 \rightarrow H_2+o\text{-}C_6H_4$:

$$k_e = l_c^{\neq} I_r \frac{kT}{h} \frac{e^{-E_b^o/RT}}{Q_{C_6H_6}} \times \int_0^{\infty} \frac{\omega_1 k_e(E) \Sigma P_c(E^{\neq})}{AB \cdot BA} e^{-E^{\neq}/RT} d\left(\frac{E^{\neq}}{RT}\right),$$

$C_6H_6 \rightarrow o\text{-}C_6H_6 \rightarrow m\text{-}C_6H_6$:

$$k_h = l_c^{\neq} I_r \frac{kT}{h} \frac{e^{-E_b^o/RT}}{Q_{C_6H_6}} \times \int_0^{\infty} \frac{\omega_1 \omega_2 GH \Sigma P_c(E^{\neq})}{AB \cdot BA} e^{-E^{\neq}/RT} d\left(\frac{E^{\neq}}{RT}\right),$$

$C_6H_6 \rightarrow o\text{-}C_6H_6 \rightarrow m\text{-}C_6H_6 \rightarrow H+C_6H_5$:

$$k_i = l_c^{\neq} I_r \frac{kT}{h} \frac{e^{-E_b^o/RT}}{Q_{C_6H_6}} \times \int_0^{\infty} \frac{\omega_1 GH \cdot k_i(E) \Sigma P_c(E^{\neq})}{AB \cdot BA} e^{-E^{\neq}/RT} d\left(\frac{E^{\neq}}{RT}\right),$$

$C_6H_6 \rightarrow o\text{-}C_6H_6 \rightarrow m\text{-}C_6H_6 \rightarrow ac\text{-}C_6H_6$:

$$k_j = l_c^{\neq} I_r \frac{kT}{h} \frac{e^{-E_b^o/RT}}{Q_{C_6H_6}} \times \int_0^{\infty} \frac{\omega_1 \omega_3 GH \cdot HG \Sigma P_c(E^{\neq})}{AB \cdot BA} e^{-E^{\neq}/RT} d\left(\frac{E^{\neq}}{RT}\right).$$

In the above equations,

$$AB = \omega_1 + k_b(E) + k_c(E) - k_c(E) k_{-c}(E)/BA,$$

$$BA = k_{-c}(E) + k_d(E) + k_f(E) - k_{-f}(E) \cdot GH,$$

$$GH = k_f(E)/(k_{-f}(E) + k_g(E) + k_i(E) + \omega_2 - k_{-g}(E) \cdot HG),$$

$$HG = k_g(E)/(k_{-g}(E) + \omega_3),$$

$$\omega_1 = k_{-a}[M], \quad \omega_2 = k_h[M], \quad \omega_3 = k_j[M],$$

where $l_x^{\neq}$, $k_x(E)$, and $\Sigma P_x(E^{\neq})$ are the statistical factor, energy-dependent specific rate constant and sum of states of the transition state for step (x) ($x=b$, c, $-c$, f, $-f$, g, $-g$, and i). E_b^0 is the C_6H_5-H dissociation energy at 0 K, $E^{\neq}$ is the excess energy above the dissociation limit, and I_r is the square-root of the ratio of the products of moments of inertia of the transition state and the reacting intermediate involved. I_r is close to unity in the present system. $Q_{C_6H_6}$ is the vibrational partition function of the C_6H_6 molecule. In our calculations of the P-dependent rate constants, the effective colli-

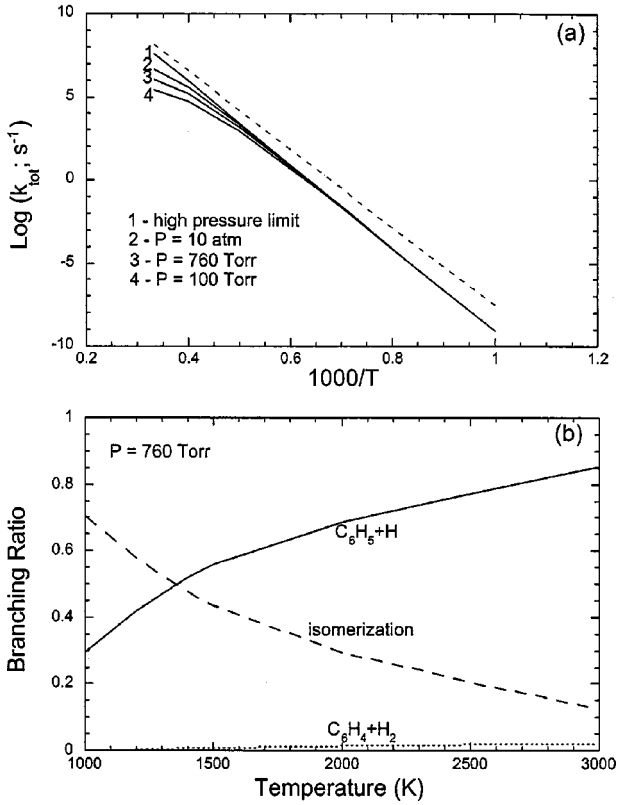

FIG. 4. (a) Arrhenius plots of total rate constants for unimolecular decomposition of benzene calculated at different pressures: curve 1, high-pressure limit; curve 2, $P=10$ atm; curve 3, $P=760$ Torr; curve 4, $P=100$ Torr. The dashed line shows recommended value for the high-pressure limit from Ref. 32. (b) Calculated branching ratios for production of $H+C_6H_5$, $C_6H_4+H_2$ and benzene isomerization as functions of temperature for $P=760$ Torr.

sion frequencies, $\omega_1-\omega_3$, evaluated with the L-J parameters[30] of C_6H_6 and Ar using Troe's weak-collision approximation,[31] were assumed to be the same. It should be mentioned that the production of p-C_6H_6 from C_6H_6 was found to be negligible [as revealed by the test replacing reaction (i) with m-$C_6H_6 \rightarrow p$-C_6H_6]; this product channel was omitted in the above analysis.

In our calculation for k_b, the rate constant for the unimolecular decomposition of C_6H_5 via step (b) producing H atoms without a well-defined transition state, we employed the maximum Gibbs free energy criterion[11,21,22] as alluded to before. The accuracy of the free energy VTST method was demonstrated by Hase and co-workers[11(d)–11(e)] by comparing its rate constant with those determined from classical trajectories for the reactions $H+CH_3 \rightarrow CH_4$ and H+diamond{111}. The potential energies of the dissociating system were calculated by full geometry optimization at different fixed C_6H_5—H separations covering from 2.0 to 3.2Å with an interval of 0.2 Å. The calculated energies at the B3LYP/6-311G(d,p) level of theory were fitted to the Morse potential and scaled to the experimental dissociation energy $D(C_6H_5-H)=113.8$ kcal/mol. For each structure, we calculated $3N-7$ vibrational frequencies projected out of the gradient direction. The energies, moments of inertia, and vibrational frequencies were used for the calculations of ΔG and finding variational transition state for each temperature. The computed variational TST rate constant, $k_b=(kT/h)\exp(-\Delta G_{\mathrm{VTS}}/RT)$, corresponding to the high pressure limit is expressed as

$$k_b = 8.43\times 10^{15}\exp(-58\,010/T)\,\mathrm{s}^{-1}$$

or

$$1.26\times 10^{18}T^{-0.59}\exp(-58\,980/T)\,\mathrm{s}^{-1}$$

for the temperatures between 1000 and 3000 K. The A-factor appears to be quite reasonable. Temperature dependence of the Arrhenius parameters is small; the deviations of the calculated parameters from those obtained in the fit are less than 7%.

The calculated total and individual rate constants for benzene decomposition and isomerization at various temperatures and pressures are collected in Table II and the Arrhenius plots showing temperature dependence of the total rate are presented in Fig. 4. k_{tot} computed for the high pressure limits exhibits a typical linear behavior (on the logarithmic scale) and can be fitted in the temperature range of 1000–3000 K by the following expression:

$$k_{\mathrm{tot}}(P=\infty)=8.75\times 10^{15}\exp(-57\,630/T)\,\mathrm{s}^{-1},$$

or

$$1.55\times 10^{12}\,T^{1.02}\exp(-55\,950/T)\,\mathrm{s}^{-1}$$

so the apparent activation energy is 115.1 kcal/mol. It is worth mentioning that this rate is slightly higher than the uncoupled high-pressure rate for the direct H loss, k_b. The deviations of k_{tot} from the Arrhenius behavior do not exceed 7%.

The rate computed for the finite pressures, 100 and 760 Torr and 10 atm, deviate from the Arrhenius behavior at high temperatures. This fall-off of the rate constant is especially large for the low pressure of 100 Torr, where the rate at 3000 K is about 150 times lower than the corresponding high-pressure limit. The 3000 K rates at $P=760$ Torr and 10 atm constitute 11.1% and 2.8%, respectively, from the high-pressure limit. A nonlinear fit of k_{tot} calculated at different pressures gives the following expressing in s^{-1} for $1000\,\mathrm{K} \leqslant T \leqslant 3000\,\mathrm{K}$:

$$k_{\mathrm{tot}}(1000\,\mathrm{Torr})=3.47\times 10^{72}\,T^{-16.03}\exp(-77\,386/T),$$

$$k_{\mathrm{tot}}(760\,\mathrm{Torr})=3.07\times 10^{57}\,T^{-11.73}\exp(-72\,466/T),$$

$$k_{\mathrm{tot}}(10\,\mathrm{atm})=3.30\times 10^{40}\,T^{-6.92}\exp(-66\,507/T).$$

For the high-pressure limit, the computed rate constant is lower by a factor of 33, 12, and 3.2 at $T=1000$, 2000, and 3000 K, respectively, than the rate recommended for H-atom production based on kinetic modeling of global experimental data,[32]

$$k_{\mathrm{exp}}=9.0\times 10^{15}\exp(-54\,060/T)\,\mathrm{s}^{-1}.$$

Possible reasons for such deviation will be discussed below.

The dependence of branching ratios for various products on the temperature at $P=760$ Torr is illustrated in Fig. 4(b). At $T=1000$ K the C_6H_5+H channel makes up only 29% of the total reaction products while the rest 71% are iso-C_6H_6,

TABLE III. Calculated total and individual rate constants for the $H+C_6H_5$ recombination reaction ($cm^3\,molecule^{-1}\,s^{-1}$) at various pressures.

T,K	k_{tot}[a]	k_{rec}[b]	k(benzene)	$k(C_6H_4+H_2)$	$k(m\text{-}C_6H_6)$	k(ac-C_6H_6)	$k(p\text{-}C_6H_6)$	k_{iso}
				$P=760$ Torr				
300	6.17×10^{-11}	6.17×10^{-11}	6.17×10^{-11}	1.97×10^{-24}	2.64×10^{-16}	1.45×10^{-16}	1.07×10^{-16}	5.15×10^{-16}
500	4.48×10^{-11}	4.48×10^{-11}	4.47×10^{-11}	6.88×10^{-21}	1.10×10^{-14}	2.43×10^{-14}	5.39×10^{-15}	4.07×10^{-14}
1000	4.54×10^{-11}	4.54×10^{-11}	4.38×10^{-11}	4.70×10^{-16}	4.17×10^{-14}	1.60×10^{-12}	1.33×10^{-14}	1.66×10^{-12}
1500	6.07×10^{-11}	5.98×10^{-11}	5.05×10^{-11}	2.22×10^{-13}	2.57×10^{-14}	9.08×10^{-12}	3.82×10^{-15}	9.11×10^{-12}
2000	9.49×10^{-11}	7.71×10^{-11}	4.32×10^{-11}	4.07×10^{-12}	3.48×10^{-14}	2.99×10^{-11}	1.07×10^{-15}	2.99×10^{-11}
2500	1.26×10^{-10}	6.07×10^{-11}	1.78×10^{-11}	1.41×10^{-11}	2.90×10^{-14}	2.88×10^{-11}	3.25×10^{-16}	2.88×10^{-11}
3000	1.46×10^{-10}	3.71×10^{-11}	3.66×10^{-12}	2.42×10^{-11}	9.36×10^{-15}	9.22×10^{-12}	8.92×10^{-17}	9.23×10^{-12}
				$P=10$ atm				
300	6.17×10^{-11}	6.17×10^{-11}	6.17×10^{-11}	1.49×10^{-24}	3.73×10^{-16}	2.31×10^{-17}	1.23×10^{-16}	5.19×10^{-16}
500	4.48×10^{-11}	4.48×10^{-11}	4.47×10^{-11}	4.26×10^{-21}	2.51×10^{-14}	6.26×10^{-15}	9.61×10^{-15}	4.10×10^{-14}
1000	4.54×10^{-11}	4.54×10^{-11}	4.37×10^{-11}	8.20×10^{-17}	2.92×10^{-13}	1.28×10^{-12}	8.91×10^{-14}	1.66×10^{-12}
1500	5.94×10^{-11}	5.93×10^{-11}	5.19×10^{-11}	3.90×10^{-14}	1.82×10^{-13}	7.09×10^{-12}	3.63×10^{-14}	7.31×10^{-12}
2000	8.72×10^{-11}	8.14×10^{-11}	5.74×10^{-11}	1.54×10^{-12}	9.85×10^{-14}	2.24×10^{-11}	1.03×10^{-14}	2.25×10^{-11}
2500	1.30×10^{-10}	9.21×10^{-11}	3.83×10^{-11}	9.39×10^{-12}	8.18×10^{-14}	4.43×10^{-11}	2.97×10^{-15}	4.43×10^{-11}
3000	1.58×10^{-10}	6.70×10^{-11}	1.28×10^{-11}	2.14×10^{-11}	4.54×10^{-14}	3.27×10^{-11}	8.27×10^{-16}	3.28×10^{-11}
				$P=100$ Torr				
300	6.17×10^{-11}	6.17×10^{-11}	6.17×10^{-11}	5.40×10^{-24}	9.01×10^{-17}	3.64×10^{-16}	5.95×10^{-17}	5.14×10^{-16}
500	4.48×10^{-11}	4.48×10^{-11}	4.47×10^{-11}	2.56×10^{-20}	2.34×10^{-15}	3.66×10^{-14}	1.53×10^{-15}	4.05×10^{-14}
1000	4.55×10^{-11}	4.55×10^{-11}	4.38×10^{-11}	3.02×10^{-15}	6.31×10^{-15}	1.75×10^{-12}	1.89×10^{-15}	1.75×10^{-12}
1500	6.38×10^{-11}	6.05×10^{-11}	4.65×10^{-11}	7.40×10^{-13}	1.08×10^{-14}	1.32×10^{-11}	5.13×10^{-16}	1.32×10^{-11}
2000	9.43×10^{-11}	5.98×10^{-11}	2.77×10^{-11}	6.88×10^{-12}	1.87×10^{-14}	2.52×10^{-11}	1.51×10^{-16}	2.53×10^{-11}
2500	1.17×10^{-10}	3.50×10^{-11}	7.24×10^{-12}	1.66×10^{-11}	8.59×10^{-15}	1.11×10^{-11}	4.58×10^{-17}	1.11×10^{-11}
3000	1.42×10^{-10}	2.79×10^{-11}	9.79×10^{-13}	2.50×10^{-11}	1.71×10^{-15}	1.98×10^{-12}	1.20×10^{-17}	1.98×10^{-12}

[a]Total rate constants including indirect redissociation to $H+C_6H_5$.
[b]Total recombination rate constant, $H+C_6H_5\rightarrow$products.

mostly ac-C_6H_6 (62%) and m-C_6H_6 (9%). With temperature increase, the branching ratio for the hydrogen elimination channel goes up and reaches 85.5% at 3000 K and the branching ratio for ac-C_6H_6 decreases to 12.3%. The $C_6H_4+H_2$ channel plays a minor role with its largest branching ratio of 2.2% at 3000 K. At different pressures (100 Torr, 10 atm and high-pressure limit) the behavior of branching ratios is qualitatively similar to that at the atmospheric pressure, although some small quantitative differences persist. For example, at the high pressure limit and 3000 K the branching ratio of m-C_6H_6 is 21% while the contribution of ac-C_6H_6 is negligible. The ratio of the H_2 lost in this case increases to 4%. At the low pressure ($P=100$ Torr) and 3000 K the branching ratios are 90.6%, 7.6%, and 1.8% for C_6H_5+H, ac-C_6H_6, and $C_6H_4+H_2$, respectively.

As one can see, the isomerization channels followed by stabilization of iso-C_6H_6, mostly ac-C_6H_6, are preferable in the unimolecular reaction of benzene at temperatures around 1000 K. On the other hand, the recommended expression for the total decomposition rate was obtained from kinetic modeling of experimental data.[32] In this modeling, a generally accepted reaction mechanism was assumed implying that the only channel of benzene decomposition is the channel yielding the $H+C_6H_5$ products. In view of our present results, the kinetic model for interpretation of experimental data on benzene unimolecular reaction should be reconsidered. In the next section we will show that the total rate of the reverse $H+C_6H_5$ reaction computed using the same potential energy surface with similar RRKM calculations is fairly close to the experimental rate measured directly. We also found another confirmation of our *ab initio*/RRKM calculations for benzene decomposition rate constants through a study of the decomposition under collision-free conditions (photodissociation in molecular beams occurring via internal conversion into the vibrationally hot ground electronic state) on the same PES. Results of this study will be published elsewhere,[33] but it is worth mentioning here that the computed lifetime of the benzene molecule for the energy corresponding to the 193 nm photoexcitation is 28.5 μs, reasonably close to the experimental lifetimes recently measured at this wavelength, 10 and 20 μs for benzene and d_6-benzene, respectively.[34]

2. Bimolecular $H+C_6H_5$ reaction

A similar scheme as shown above for the decomposition reaction was established for $H+C_6H_5$ by steady-state treatment for all excited isomers of C_6H_6. The scheme and rate constant expressions are omitted here for brevity.

Table III presents total and individual rate constants for the $H+C_6H_5$ recombination reaction calculated at various pressures. Figure 5(a) shows Arrhenius plots of these rates for the atmospheric pressure in the temperature range of 300–3000 K. For $T<2000$ K, the total recombination rate varies in the range of $4.3–7.7\times10^{-11}\,cm^3\,molecule^{-1}\,s^{-1}$ and the reaction is dominated by the formation of benzene. A slight negative temperature dependence is found between 300 and 800 K, where k_{rec} decreases from 6.17×10^{-11} to $4.35\times10^{-11}\,cm^3\,molecule^{-1}\,s^{-1}$. At $T\geqslant2000$ K, the reaction channels resulting in indirect redissociation to C_6H_5+H, for example, via C_6H_6 **1**$\rightarrow o$-C_6H_6, **2**$\rightarrow C_6H_5+H$, substantially contribute to the reaction, so the apparent recombination rate k_{rec} is lower than the total rate constant [curve 1 in Fig. 5(a)].

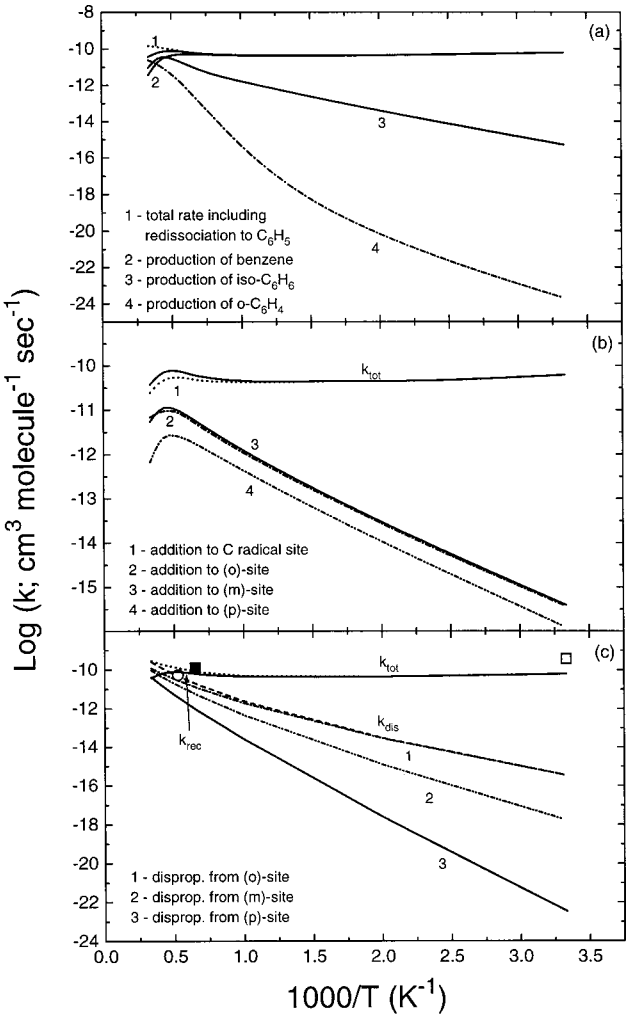

FIG. 5. (a) Arrhenius plots of total, net recombination and individual rate constants for the $H+C_6H_5$ recombination reaction. Curve 1 shows the total rate including indirect redissociation back to the reactants. Curves 2, 3, and 4 correspond to the production of benzene, iso-C_6H_6, and o-$C_6H_4+H_2$, respectively. (b) Arrhenius plots of the total rate (k_{tot}) and individual rate of different incoming channels of the $H+C_6H_5$ recombination reaction: curve 1, H addition to the radical site; curve 2, H addition to *o*-site; curve 3, H addition to *m*-site; curve 4, H addition to *o*-site. (c) Arrhenius plots of rate constants for various H disproportionation channels to *o*-position (dashed curve 1), *m*-position (dashed curve 2), and *p*-position (dashed curve 3), the total disproportionation rate constant k_{dis}, the total recombination rate constant k_{rec} computed for $P=760$ Torr, and the total rate of the bimolecular $H+C_6H_5$ reaction, $k_{tot}=k_{dis}+k_{rec}$. Circle, Ref. 35; open square, Ref. 36, and filled rectangle, Ref. 37.

At $T=1200$ K a contribution of the ac-C_6H_6 product channel becomes substantial, about 7% of the total recombination rate. The ac-C_6H_6 branching ratio increases to 39% at $T=2000$ K, while that of benzene formation is down to 56%. The rate constant for the $C_6H_4+H_2$ product channel exhibits the strongest positive temperature dependence. As a result, the H_2 elimination channels becomes major at $T=3000$ K, 65% vs 25% and 10% for the production of ac-C_6H_6 and benzene, respectively.

The total recombination rate k_{rec} is virtually pressure independent at T below 1500 K. However, some differences are seen at higher temperatures. For example, at 3000 K k_{rec} computed for 100 Torr, 760 Torr, and 10 atm constitute 20%, 26%, and 47%, respectively, of the high pressure limit rate constants. At the high pressure limit, the rates for the benzene and ac-C_6H_6 reaction channels do not show the high-temperature fall-off behavior. The fall-off differs at different pressures. Hence, the branching ratios at 3000 K significantly depend on the pressure. For instance, the respective branching ratios of benzene, iso-C_6H_6, and $C_6H_4+H_2$ are 60.1%, 39.5%, and 0.4% at the high pressure limit. Under high pressure conditions, once an intermediate is formed it tends to be rapidly stabilized by the collisional energy transfer. Therefore, the 3000 K branching ratio of ac-C_6H_6 is nearly zero, while those for m-C_6H_6 and p-C_6H_6 increase to 28.8% and 10.7%, respectively. At $P=10$ atm and 3000 K, the channel producing ac-C_6H_6 is major in the recombination reaction with the branching ratio of 49%, while the branching ratios for the formation of benzene and $C_6H_4+H_2$ are 19% and 32%, respectively. At the low pressure of 100 Torr and high temperatures, the formation of $C_6H_4+H_2$ is more significant than at the atmospheric pressure. The 3000 K branching ration of this channel is 89.4% vs 3.5% and 7.1% for the formation of benzene and ac-C_6H_6, respectively.

It is also interesting to compare the individual rate constants of four different incoming channels, H addition to the C· radical site as well as H addition to CH groups in *o*-, *m*-, and *p*-positions. The rates computed for $P=760$ Torr are shown in Fig. 5(b). The addition to the radical site dominates the reaction in the whole 300–3000 K temperature range showing a slight negative temperature dependence and a fall-off at $T>2000$ K (curve 1). The H additions to CH groups have distinct barriers of about 6 kcal/mol, so they mostly demonstrate a linear positive temperature dependence (curves 2–4). At $T=3000$ K, the rate of the addition channel to the radical site is equal to 78% of the total reaction rate constant and the fractions of the *o*- and *m*-additions are 11% and 10%, respectively. The rate for *p*-addition at 300 K $\leqslant 1500$ K T is about 3 times slower than those for the *o*- and *m*-additions. This result is related to slightly higher barrier for the *p*-addition, but mostly due to the lower symmetry factor and a tighter structure of the transition state.

Figure 5(c) shows Arrhenius plots of the rates for various *H* disproportionation channels leading to the *o*-, *m*-, or p-$C_6H_4+H_2$ products, the total rate for the three disproportionation channels, k_{dis}, and the total rate of the bimolecular $H+C_6H_5$ reaction, $k_{tot}=k_{rec}+k_{dis}$, where k_{rec} is computed at the atmospheric pressure. The values of these rate constants at various temperatures in the 300–3000 K range are collected in Table IV. Among the disproportionation channels, the one leading to o-$C_6H_4+H_2$ is the most significant since it has the lowest barrier, 7.6 kcal/mol. Below 2000 K, the bimolecular reaction is dominated by the recombination processes, but at $T>2200$ K H-disproportionation takes over. The k_{dis}/k_{tot} and k_{rec}/k_{tot} ratios are 68.7% and 31.3% at 2500 K and 87.0% and 13.0% at 3000 K, respectively. Taking into account that the recombination reaction at high temperatures is also dominated by the H_2 loss channel we can conclude that o-benzyne$+H_2$ should be the major reaction products at $T=2500$ K and higher.

Three more direct (less convoluted) experimental measurements of the rate constant for $H+C_6H_5$ are available

TABLE IV. Calculated rate constants for various H disproportionation channels and total rate constants of the bimolecular $H+C_6H_5$ reaction ($cm^3\,molecule^{-1}\,s^{-1}$).

T,(K)	$k(o\text{-}C_6H_4)$	$k(m\text{-}C_6H_4)$	$k(p\text{-}C_6H_4)$	k_{dis}[a]	k_{tot}[b]
300	3.38×10^{-16}	1.67×10^{-18}	3.39×10^{-23}	3.39×10^{-16}	6.17×10^{-11}
500	2.83×10^{-14}	1.22×10^{-15}	2.49×10^{-18}	2.95×10^{-14}	4.48×10^{-11}
1000	1.91×10^{-12}	4.59×10^{-13}	2.51×10^{-14}	2.40×10^{-12}	4.78×10^{-11}
1500	1.15×10^{-11}	4.93×10^{-12}	7.81×10^{-13}	1.72×10^{-11}	7.70×10^{-11}
2000	3.32×10^{-11}	1.91×10^{-11}	5.10×10^{-12}	5.74×10^{-11}	1.35×10^{-10}
2500	6.87×10^{-11}	4.73×10^{-11}	1.72×10^{-11}	1.33×10^{-10}	1.94×10^{-10}
3000	1.18×10^{-10}	9.16×10^{-11}	4.08×10^{-11}	2.51×10^{-10}	2.88×10^{-10}

[a]Total rate three H disproportionation channels, $k_{dis}=k(o\text{-}C_6H_4)+k(m\text{-}C_6H_4)+k(p\text{-}C_6H_4)$.
[b]Total rate for the bimolecular $H+C_6H_5$ reaction, $k_{tot}=k_{dis}+k_{rec}$, where k_{rec} is taken for $P=760$ Torr (see Table III).

in the literature.[35–37] Troe and co-workers reported the values of $5.2\times10^{-11}\,cm^3\,molecule^{-1}\,s^{-1}$ for the temperaure range of 1600–2100 K at 560 Torr Ar (Ref. 35) and $3.7\times10^{-10}\,cm^3\,molecule^{-1}\,s^{-1}$ at 300 K for 74–750 Torr Ar,[36] while Braun-Unkhoff *et al.*[37] obtained $1.3\times10^{-10}\,cm^{-3}\,molecule^{-1}\,s^{-1}$ for $1380\,K\leqslant T\leqslant1700\,K$, 1.13×10^{3} Torr $\leqslant P(Ar)\leqslant4.55\times10^{3}$ Torr. The latter value is recommended as preferred.[32] As seen in Fig. 5(c), our theoretical results for the bimolecular $H+C_6H_5$ reaction, although are in good accord with the value of Troe *et al.*, are about 40% lower than the measurement by Braun-Unkhoff *et al.*[37] At $T=1500\,K$, the computed rate constant is $7.70\times10^{-11}\,cm^3\,molecule^{-1}\,s^{-1}$. It is interesting to mention that about 22% of the total rate at this temperature is due to the hydrogen disproportionation channels which were, however, not included in the kinetic modeling of high-temperature shock tube data. The deviation of the calculated values from experiment, therefore, may be due in part to the omission and in part to the possibility that the recombination reaction can also occur in the triplet electronic state initially forming triplet benzene. The role of the T_1 state of C_6H_6 in the $H+C_6H_5$ reaction and unimolecular decomposition of benzene will be a subject of our future investigations.

IV. CONCLUDING REMARKS

Ab initio G2M(cc, MP2) calculations of the potential energy surface of unimolecular decomposition of benzene and bimolecular $H+C_6H_5$ reaction show that the reactions can occur by various mechanisms. Besides direct emission of a hydrogen atom taking place without exit barrier, benzene molecule can undergo sequential 1,2-hydrogen shifts to *o*-, *m*-, and *p*-C_6H_6 and then lose a H atom with exit barriers of about 6 kcal/mol. *o*-C_6H_6 **2** can eliminate a hydrogen molecule with a barrier of 121.4 kcal/mol relative to benzene. *o*- and *m*-C_6H_6 **4** can also isomerize to acyclic isomers ac-C_6H_6, **3** and **3′**, with barriers of 110.7 and 100.6 kcal/mol, respectively. However, in order to form *m*-C_6H_6 from benzene the system has to overcome a barrier of 108.6 kcal/mol for the 1,2-H migration from *o*-C_6H_6 to *m*-C_6H_6.

The bimolecular $H+C_6H_5$ reaction is shown to be far more complicated than the unimolecular fragmentation reaction because of the presence of various metathetical processes, such as H-atom disproportionation or addition to different sites of the ring. The addition to the radical site is barrierless but the other three channels of hydrogen addition to the phenyl radical, to the *o*-, *m*-, and *p*-positions, have entrance barriers of about 6 kcal/mol and can interact with each other through hydrogen shifts in *o*-, *m*-, and *p*-C_6H_6 because the energies of transition states for the H migrations are lower than that of $H+C_6H_5$. Among the disproportionation channels, the one leading to *o*-benzyne$+H_2$ is the most significant, since it has the lowest barrier of 7.6 kcal/mol.

Using the RRKM and TST methods we were able to compute the total and individual rate constants for various channels of benzene unimolecular decomposition and $H+C_6H_5$ reaction under different temperature/pressure conditions. Two- and three-parameter fits of the calculated rates gave the following expression for the total rate constant for benzene fragmentation for the temperature range of 1000–3000 K and atmospheric pressure:

$$k_{tot}(760\,Torr)=3.07\times10^{57}T^{-11.73}\exp(-72\,470/T)\,s^{-1}$$

or

$$\sim2.3\times10^{14}\exp(-53300/T)\,s^{-1}.$$

Theoretical values of k_{tot} are 3–30 times lower than the values recommended earlier[32] based on kinetic modeling of experimental measurements assuming *only* the H-atom production channel. Our present results show that at 1000 K the branching ratio of the $H+C_6H_5$ products, generally assumed to be the dominant reaction products, is only 29%, while the major reaction channel is the benzene isomerization to ac-C_6H_6. Therefore, the kinetic model for benzene unimolecular decomposition should be reconsidered. The $C_6H_4+H_2$ products are demonstrated to play a minor role in the thermal decomposition reaction.

The total rate for the bimolecular $H+C_6H_5$ reaction is predicted to be 4.5×10^{-11}–$2.9\times10^{-10}\,cm^3\,molecule^{-1}\,s^{-1}$ for the broad range of temperatures (300–3000 K) and pressures (100 Torr–10 atm). The computed rate at 1500 K underestimates the recommended value, $1.3\times10^{-10}\,cm^3\,molecule^{-1}\,s^{-1}$ measured for the temperature interval of 1380–1700 K,[37] by ~40%. The recombination reaction, dominated by direct formation of benzene molecule through H addition to the radical site, is more important than H disproportionations at $T<2000\,K$. At higher temperatures, the recombination channel leading to $C_6H_4+H_2$ and hydrogen disproportionation channels become more significant

and *o*-benzyne+H_2 should be the major reaction products at $T>2500$ K. These product channels were not considered in the kinetic modeling of high-temperature shock tube data. This and the possibility of the T_1-state involvement at high temperatures may account for the deviation mentioned above.

ACKNOWLEDGMENTS

This work was supported in part by Academia Sinica and by the Petroleum Research Fund, ROC. The work carried out at Emory University was supported by the Basic Energy Sciences, Division of Chemical Sciences, the U.S. Department of Energy, under Contract No. DE-FG02-97-ER14784.

[1] I. Glassman, *Combustion*, 2nd ed. (Academic, New York, 1987).
[2] N. Fujii and T. Asaba, 14th Symp. (Int.) Combust. **433**, (1972).
[3] N. Fujii and T. Asaba, J. Fac. Eng. Tokyo Ser. B **34**, 189 (1977).
[4] H. J. Singh and R. D. Kern, Combust. Flame **54**, 49 (1983).
[5] V. S. Rao and G. B. Skinner, J. Phys. Chem. **88**, 5990 (1984).
[6] R. D. Kern, C. H. Wu, G. B. Skinner, V. S. Rao, J. H. Kiefer, J. A. Towers, and L. J. Mizerka, 20th Symp. (Int.) Combust. **789**, (1984).
[7] D. S. Hsu, C. Y. Lin, and M. C. Lin, 20th Symp. (Int.) Combust. **623**, (1984).
[8] J. H. Kiefer, L. J. Mizerka, M. R. Patel, and H. C. Wei, J. Phys. Chem. **89**, 2013 (1985).
[9] V. S. Rao and G. B. Skinner, J. Phys. Chem. **92**, 2442 (1988).
[10] A. Yokoyama, X. Zhao, E. J. Hintsa, R. E. Continetty, and Y. T. Lee, J. Chem. Phys. **92**, 4222 (1990).
[11] (a) W. L. Hase, J. Chem. Phys. **64**, 2442 (1976); (b) B. C. Garret and D. G. Truhlar, *ibid.* **70**, 1593 (1979); (c) A. D. Isaacson and D. G. Truhlar, *ibid.* **76**, 1380 (1982); (d) X. Hu and W. L. Hase, *ibid.* **95**, 8073 (1991); (e) K. Song, P. d. Sainte Claire, W. L. Hase, and K. C. Hass, Phys. Rev. B **52**, 2949 (1995).
[12] (a) A. D. Becke, J. Chem. Phys. **98**, 5648 (1993); (b) C. Lee, W. Yang, and R. G. Parr, Phys. Rev. B **37**, 785 (1988).
[13] W. J. Hehre, L. Radom, P. v. R. Schleyer, and J. A. Pople, *Ab Initio Molecular Orbital Theory* (Wiley, New York, 1986).
[14] L. K. Madden, A. M. Mebel, M. C. Lin, and C. F. Melius, J. Phys. Org. Chem. **9**, 801 (1996).
[15] H. F. Bettinger, P. R. Schreiner, P. v. R. Schleyer, and H. F. Schaefer, J. Phys. Chem. **100**, 16147 (1996).
[16] A. M. Mebel, K. Morokuma, and M. C. Lin, J. Chem. Phys. **103**, 7414 (1995).
[17] (a) L. A. Curtiss, K. Raghavachari, G. W. Trucks, and J. A. Pople, J. Chem. Phys. **94**, 7221 (1991); (b) J. A. Pople, M. Head-Gordon, D. J. Fox, K. Raghavachari, and L. A. Curtiss, *ibid.* **90**, 5622 (1989); (c) L. A. Curtiss, C. Jones, G. W. Trucks, K. Raghavachari, and J. A. Pople, *ibid.* **93**, 2537 (1990).
[18] (a) G. D. Purvis and R. J. Bartlett, J. Chem. Phys. **76**, 1910 (1982); (b) C. Hampel, K. A. Peterson, and H.-J. Werner, Chem. Phys. Lett. **190**, 1 (1992); (c) P. J. Knowles, C. Hampel, and H.-J. Werner, J. Chem. Phys. **99**, 5219 (1994); (d) M. J. O. Deegan and P. J. Knowles, Chem. Phys. Lett. **227**, 321 (1994).
[19] M. J. Frisch, G. W. Trucks, H. B. Schlegel *et al.*, GAUSSIAN 94, Revision E.2, Gaussian, Inc., Pittsburgh, Pennsylvania, 1995.
[20] MOLPRO is a package of *ab initio* programs written by H.-J. Werner and P. J. Knowles, with contributions from J. Almlöf, R. D. Amos, M. J. O. Deegan, S. T. Elbert, C. Hampel, W. Meyer, K. Peterson, R. Pitzer, A. J. Stone, P. R. Taylor, and R. Lindh.
[21] C.-C. Hsu, A. M. Mebel, and M. C. Lin, J. Chem. Phys. **105**, 2346 (1996).
[22] A. M. Mebel, E. W. G. Diau, M. C. Lin, and K. Morokuma, J. Am. Chem. Soc. **118**, 9759 (1996).
[23] D. S. Y. Hsu, W. M. Shaub, T. Creamer, D. Gutman, and M. C. Lin, Ber. Bunsenges. Phys. Chem. **87**, 909 (1983).
[24] G. E. Davigo, V. Bierbaum, C. H. DePuy, G. B. Ellison, and R. R. Squires, J. Am. Chem. Soc. **117**, 2590 (1995).
[25] (a) A. H. H. Chang, A. M. Mebel, X.-M. Yang, S. H. Lin, and Y. T. Lee, Chem. Phys. Lett. **287**, 301 (1998); J. Chem. Phys. **109**, 2748 (1998).
[26] A. M. Mebel, S. H. Lin, X.-M. Yang, and Y. T. Lee, J. Phys. Chem. A **101**, 6781 (1997).
[27] A. M. Mebel, M. C. Lin, T. Yu, and K. Morokuma, J. Phys. Chem. A **101**, 3189 (1997).
[28] (a) P. G. Wenthold, J. A. Paulino, and R. R. Squires, J. Am. Chem. Soc. **113**, 7414 (1991); (b) P. G. Wenthold and R. R. Squires, *ibid.* **116**, 6401 (1994); (c) R. Lindh, T. J. Lee, A. Bernhardsson, B. J. Persson, and G. Karlström, *ibid.* **117**, 7186 (1995); (d) L. V. Moskaleva, L. K. Madden, and M. C. Lin, Phys. Chem. Chem. Phys. **1**, 3967 (1999).
[29] C. F. Logan and P. Chen, J. Am. Chem. Soc. **118**, 2113 (1996).
[30] L. I. Stiel and G. Thodos, J. Chem. Eng. Data **7**, 234 (1962).
[31] J. Troe, J. Phys. Chem. **83**, 114 (1979).
[32] D. L. Baulch, C. J. Cobos, R. A. Cox, C. Esser, P. Franck, Th. Just, J. A. Kerr, M. J. Pilling, J. Troe, R. W. Walker, and J. Warnatz, J. Phys. Chem. Ref. Data **21**, 411 (1992).
[33] A. M. Mebel, A. H. H. Chang, and S. H. Lin (to be published).
[34] S.-T. Tsai, C.-K. Lin, Y. T. Lee, and C.-K. Ni, J. Chem. Phys. **113**, 67 (2000).
[35] W. Muller-Markgraf and J. Troe, J. Phys. Chem. **92**, 4914 (1988).
[36] L. Ackermann, H. Hippler, and P. Pagsberg, C. Reihs, and J. Troe, J. Phys. Chem. **94**, 5247 (1990).
[37] M. Braun-Unkhoff, P. Frank, and Th. Just, 22th Symp. (Int.) Combust. **1053**, (1989).